Adaptive Backstepping Sliding Mode Control for 3-DOF Permanent Magnet Spherical Actuator

Jingmeng Liu, Huiyang Deng, Cungang Hu, Zhiquan Hua, Weihai Chen*, *Member*, *IEEE*

Abstract

In this paper, a robust adaptive control system combining backstepping and sliding mode control method has been implemented for the 3-DOF permanent magnet (PM) spherical actuator in order to improve its trajectory tracking performance. Due to the complexity of both mechanical structure and electromagnetic field, the dynamic model of a PM spherical actuator inevitably contains uncertainties, such as disturbances and model errors, which will gravely influence the performance of conventional control system. Therefore, a backstepping sliding mode approach is firstly applied, where the backstepping design is to synthesise the controller and the sliding mode term is to compensate disturbances. Then, an adaptive law is presented to estimate the model errors during the control process, where the parameters of the model are initially assumed to be accuracy. Correspondingly, the stability can be guaranteed by choosing the appropriate Lyapunov function. Both simulations and experiments are designed to demonstrate the effectiveness of the proposed control scheme.

Index Terms

Spherical actuator, robust adaptive control, back-stepping control, sliding mode control, uncertainty compensation

I. Introduction

With the development of modern industrial technology, the demand for a multiple-degree-of-freedom (multiple-DOF) actuator is increasing considerably on many occasions. Conventionally, these multiple-DOF actuators are realized by connecting several single-axis motors in parallel or in series, which inevitably results in problems such as slow dynamic response, low positioning precision and lack of dexterity. In contrast, a spherical actuator can offer the same motion capacity as the conventional one, which overcomes these disadvantages and even makes the design become much simpler and clearer (Hey et al. [2014], Lee and Sosseh [2002]).

So far, spherical actuators with various structures and working principles have been proposed. In this paper, we focus on the permanent magnet (PM) spherical actuator because of its simple structure, high flux density and rapid response (Son and Lee [2010]). In our previous work, we designed this kind of spherical actuator that can realize spinning and tilting motion, and the orientation can be measured through a novel spherical joint (Chen et al. [2012]).

Since applications of the spherical actuator always involve trajectory tracking, many control methods have been developed for this. The proportional derivative (PD) control scheme is a typical feedback control approach, which has the advantage of simplicity in both design and implementation (Ackermann et al. [2004], Maeda et al. [2010], Son and Lee [2014]). However, the performance of the PD control scheme will be unsatisfactory in high accuracy occasion, since there always exist nonlinearities and uncertainties in the dynamic model. In Wang et al. [2003], Lee et al. [1996], the computed torque method (CTM) is proposed to linearize and decouple the dynamics of a PM spherical motor, but it also can not get acceptable results when the system is subjected to model errors and various external disturbances. In order to make suitable compensation for these uncertainties, intelligent control schemes have been employed in recent years. The neural networks (NNs) can handle complicated dynamic systems and are capable of learning and adaptability (Xia et al. [2010], Li [2009]). However, NNs require large training data and face difficulties in fast convergence, which limits their application for the real-time control of the PM spherical actuator.

These issues motivated us to design a control scheme that can cope with modeling errors, load variations and other disturbances of the PM spherical actuator in real time. Backstepping is a systematic and recursive design methodology for nonlinear control applied to the feedback-linearizable system, which can guarantee global regulation and tracking performance (Bin et al. [2006], Zhou et al. [2004]). The overall system is partitioned into several subsystems with lower dimension, for which select appropriate functions of state variables as pseudocontrol inputs according to corresponding Lyapunov function recursively. Each backstepping stage involves a new pseudocontrol design, expressed in terms of the one from the preceding design stage. When the procedure terminates, the true control input can be obtained with the help of Lyapunov function, which is formed by summing up the individual one associated with corresponding design stage (Maneeratanaporn et al. [2010], Madani and Benallegue [2006]). Further, the variable structure control strategy using the slide mode has been the focus of much research, as this approach is insensitive to parameter variations and disturbances (Utkin et al. [2009], Lee et al. [2009]). In general, the control process of a sliding mode controller can be divided into two phase, the hitting phase and the sliding phase, according to whether all the states have reached the switching hyperplane (sliding surface). It is provable that the system will be stable and independent from uncertainties when it enters into the sliding surface. In this paper, an adaptive backstepping

*Corresponding author. e-mail: whchenbuaa@126.com,
Tel:+86 010 82315920.

sliding mode controller, which combines the merits of both backstepping control and sliding mode control (Yu et al. [2012], Lin et al. [2007, 2002]), is proposed to achieve high tracking performance. According to the Lyapunov stability theorem, the employed adaptive backstepping sliding mode controller can guarantee closed-loop stability. Furthermore, the sliding mode technique makes the system unacted on disturbances. Specifically, an adaptive law is introduced to approximate uncertainties of the dynamics online.

The reminder of this paper is organized as follows. Section II presents the dynamic model and the torque model of our PM spherical actuator. Section III introduces the controller design and analyzes the stability of the closed-loop system. Section IV and Section V present the simulations and experiments, respectively. Finally, the concluding remarks are summarized in Section VI.

II. Dynamic and Torque Model of PMSA

A. Mechinical structure and working principle

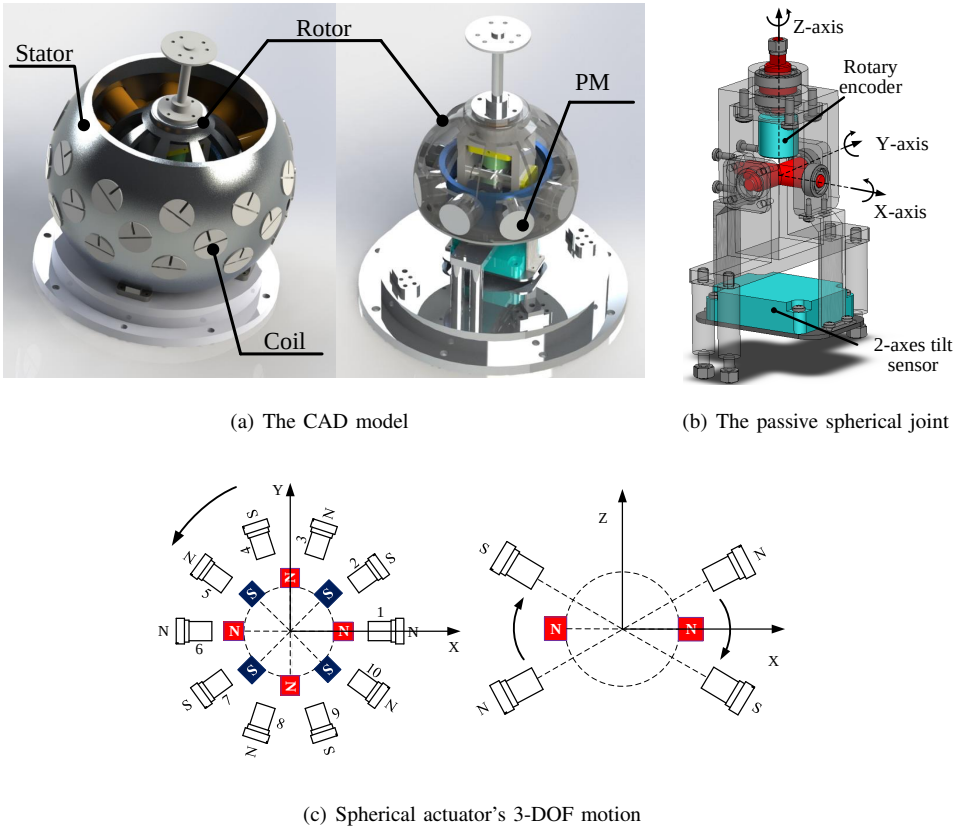

(a) The CAD model

(b) The passive spherical joint

(c) Spherical actuator's 3-DOF motion

Fig. 1. Brief introduction of the spherical actuator

The CAD model of the PM spherical actuator is shown in Fig. 1(a). The spherical actuator mainly consists of a rotor, a stator and a passive spherical joint. There are 8 PM poles arranged along the equatorial plane of the rotor and 30 coils distributed in three layers symmetrically about the equatorial plane of the stator. The passive spherical joint is shown in Fig. 1(b), including a 2-axis tilt sensor and a rotary encoder for measuring the orientation of the rotor, which serves as a basis for the closed-loop system. Additionally, this joint also acts as the support of the rotor for achieving 3-DOF motion.

Fig. 1(c) shows the fundamental working principle of spinning motion and tilting motion. When the currents of the stator coils are activated by a specific approach, the rotor can be driven by the electromagnetic force between stator coils and PM poles to realize corresponding motion.

B. Dynamic model

Euler angles (α, β, γ) are used to express the orientation of the rotor. Fig. 2 shows the coordinate transformation from the stator coordinate system to the rotor coordinate system. The rotation matrix R_{rs} is given by

$$R_{\mathrm{rs}} = \begin{bmatrix} c\beta c\gamma & -c\beta s\gamma & s\beta \\ c\gamma s\alpha s\beta + c\alpha s\gamma & c\alpha c\gamma - s\alpha s\beta s\gamma & -c\beta s\alpha \\ -c\gamma s\alpha s\beta + s\alpha s\gamma & c\gamma s\alpha + c\alpha s\beta s\gamma & c\alpha c\beta \end{bmatrix}$$

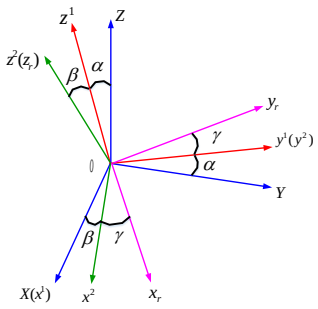

Fig. 2. Coordinate transformation

where c and s represent cosine and sine, respectively.

The dynamic model of the PM spherical actuator can be derived using the Lagrange equation as follows:

$$M(q)\ddot{q} + C(\dot{q}, q)\dot{q} = T_c - \tau_d - \tau_l \tag{1}$$

where $M(q)$ is the inertial matrix; $C(\dot{q}, q)$ is the Coriolis matrix; q $=[\alpha, \beta, \gamma]^T$ denotes the Euler angles; $T_c = \begin{bmatrix} T_x & T_y & T_z \end{bmatrix}^T$ is the control torque; τ_d is the external disturbance torque; τ_l is the load torque; The principal inertial moments of the rotor are $J_1 = J_{xx} = 2.219e-003(kg \cdot m^2)$, $J_2 = J_{yy} = 2.176e-003(kg \cdot m^2)$, $J_3 = J_{zz} = 2.256e-003(kg \cdot m^2)$.
The form of M is as follows:

$$M = \begin{bmatrix} J_1c^2\beta c^2\gamma + J_2c^2\beta s^2\gamma + J_3s^2\beta & (J_1 - J_2)c\beta c\gamma s\gamma & J_3s\beta \\ (J_1 - J_2)c\beta c\gamma s\gamma & J_1s^2\gamma + J_1c^2\gamma & 0 \\ J_3s\beta & 0 & J_3 \end{bmatrix}$$

Considering the modeling error, which cannot be prevented during the dynamic modeling process, the dynamic model can be rewritten as

$$\hat{M}(q)\ddot{q} + \hat{C}(\dot{q}, q)\dot{q} = \hat{T}_c - \tau_d - \tau_l \tag{2}$$

where $\hat{M}(q) = M(q) + \Delta M(q)$ is the actual inertial matrix and $\hat{C}(q, \dot{q}) = C(q, \dot{q}) + \Delta C(q, \dot{q})$ is the actual Coriolis matrix.

C. Torque model

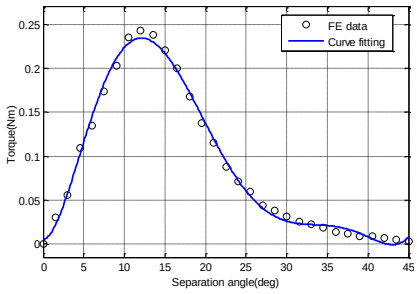

Fig. 3. Torque between a PM pole and a coil

The torque model expresses the relationship between the coil currents and the output torque at a specific rotor orientation. Fig. 3 shows the varying torque between one coil and one PM pole when the current is set as 3A, using the finite element (FE) method established in Maxwell 3-D. The horizontal axis stands for the separation angle $\varphi_{i,j}$ between the axis of ith PM pole and the axis vector of jth coil. When the value of the separation angle is 0, it means the axis vector of ith PM pole and the axis vector of jth coil have been overlapped. Then, we can keep the pole stationary and get the coil rotate around the Z axis of rotator frame to change the separation angle, and thus measuring out different torque values under these different separation angles. The torque function $f(\varphi_{i,j})$ can be obtained by utilizing the least square method based on the FE computed data, describing that the torque generated by ith PM pole and jth coil is closely linked to the relative position of the pole and the coil.

After gaining $\varphi_{i,j}$ and its corresponding $f(\varphi_{i,j})$, the torque matrix of the ith rotor pole g_i, can be derived as the following form:

$$g_i = [f(\varphi_{i,1}) \cdot d_{i,1}, f(\varphi_{i,2}) \cdot d_{i,2}, ..., f(\varphi_{i,15}) \cdot d_{i,15}] \in R^{3\times 15} \tag{3}$$

where $d_{i,j}$ represents the direction of the torque generated by the interaction of ith PM pole and jth coil. Since g_i is obtained from $f(\varphi_{i,j})$, the value of g_i is not fixed for each desired position. Conversely, its value will change with the position.

Since air-core coils are used in PM spherical actuator, the torque has a linear relationship with respect to the current. The torque model can be obtained by summing up the torques generated by all the coils using the linear superposition principle (Chen et al. [2012]), which can be expressed as

$$T = \begin{bmatrix} T_x \\ T_y \\ T_z \end{bmatrix} = GI = \begin{bmatrix} g_1 & g_2 & \dots & g_n \end{bmatrix} \begin{bmatrix} I_1 \\ I_2 \\ \dots \\ I_n \end{bmatrix} \tag{4}$$

where T is the torque; G is the torque matrix; $g_i \in R^{3\times 1}$ is the torque coefficient, which describes the torque contribution matrix of the i^{th} coil at a specific rotor orientation; I is the current of the coils; I_j is the current input of the j^{th} coil; n is the number of coils, the value of which is 15.

Given desired control torque T_c at a specific rotor orientation, we can express the current of the coils I as

$$I{=}G^T(GG^T)^{-1}T_c \tag{5}$$

However, owing to the sophisticated electromagnetic field, it is difficult to get accurate relationship between the torque and the current, resulting in a torque error τ_T. Therefore, the actual control torque $\hat{T}_{\mathrm{c}}$ can be rewritten as

$$\hat{T}_{\mathrm{c}} = T_{\mathrm{c}} - \tau_T \tag{6}$$

III. Adaptive Backstepping Sliding Mode Control

To quatify the modeling errors, the actual inertial matrix and actual Coriolis matrix are respectively redefined as

$$\hat{M}(q) = M(q) + k_1 M(q) \tag{7}$$

$$\hat{C}(\dot{q}, q) = C(\dot{q}, q) + k_2 C(\dot{q}, q) \tag{8}$$

Where k_1 and k_2 are the coefficients of the linear modeling errors. In the actual system, these two parameters are bounded as $-1 < k_1, k_2 < 1$.

To further simplify the model, we can define

$$\begin{cases} 1 + k_1 = \dfrac{1}{k_M} \\ 1 + k_2 = k_C \end{cases} \tag{9}$$

Then, the dynamic model can be rewritten as

$$\frac{1}{k_M}\hat{M}(q)\ddot{q} + k_C\hat{C}(\dot{q}, q)\dot{q} = \hat{T}_c - \tau \tag{10}$$

where $\tau = \tau_d + \tau_l + \tau_T = [\tau_x, \tau_y, \tau_z]^T$ is the lumped disturbance torque.

To handle the above lumped disturbance of the PM spherical actuator system, a hybrid controller of backstepping and sliding mode is designed to achieve the trajectory-tracking objective. As this control scheme is based on the Lyapunov function, the stability of the closed-loop system can be ensured. In addition, an adaptive method is employed to estimate the unknown parameters (k_M, k_C) in the real time.

The control strategy is described step-by-step as follows.

Step 1: Set $x_1 = q, x_2 = \dot{q}$, the state equation of the system can be expressed as

$$\begin{cases} \dot{x}_1 = x_2 \\ \dot{x}_2 = k_M\hat{M}(q)^{-1}(\hat{T}_c - \tau - k_C\hat{C}(\dot{q}, q)) \end{cases} \tag{11}$$

Take q_d as the desired trajectory, then we can define the trajectory tracking error (the error of first-order subsystem) as

$$e_1 = q - q_d \tag{12}$$

The derivative of e_1 is

$$\dot{e}_1 = \dot{q} - \dot{q}_d \tag{13}$$

The virtual controller is chosen as

$$\alpha = Ke_1 \tag{14}$$

where $K \in R^{3\times 3}$ is a positive definite diagonal coefficient matrix. The first Lyapunov function V_1 is chosen as

$$V_1 = \frac{1}{2}{e_1}^T e_1 \tag{15}$$

Define the error of second-order system as $e_2 = \dot{e}_1 + \alpha$, then the derivative of V_1 is

$$\dot{V}_1 = {e_1}^T \dot{e}_1 = {e_1}^T (e_2 - \alpha) = {e_1}^T (e_2 - K e_1) \tag{16}$$

Step 2: The derivative of e_2 is now expressed as

$$\dot{e}_2 = \ddot{e}_1 + \dot{\alpha} = \ddot{q} - \ddot{q}_d + K\dot{e}_1 \tag{17}$$

In order to design the backstepping control system, τ is assumed to be bounded as $\tau_{\max} = \{\tau_x, \tau_y, \tau_z\} \leq \tau_b$. The second Lyapunov function V_2 is chosen as follows

$$V_2 = V_1 + \frac{1}{2} s^T s \tag{18}$$

where s is the sliding surface with the form

$$s = \lambda e_1 + e_2 \tag{19}$$

where $\lambda \in R^{3\times 3}$ is a positive definite diagonal coefficient matrix. Then the derivative of V_2 can be derived as

$$\begin{aligned}
\dot{V}_2 &= \dot{V}_1 + s^T \dot{s} = e_1^T e_2 - e_1 K e_1 + s^T (\lambda \dot{e}_1 + \dot{e}_2) \\
&= e_1^T e_2 - e_1 K e_1 + s^T [\lambda (e_2 - K e_1) + \ddot{q} - \ddot{q}_d + K\dot{e}_1] \\
&= e_1^T e_2 - e_1 K e_1 + s^T [\lambda (e_2 - K e_1) + k_M \hat{M}(q)^{-1} (\hat{T}_c - \tau - k_C \hat{C}(\dot{q}, q)\dot{q}) - \ddot{q}_d + K\dot{e}_1] \\
&= e_1^T e_2 - e_1 K e_1 + s^T [\lambda (e_2 - K e_1) + k_M \hat{M}(q)^{-1} \hat{T}_c - k_M \hat{M}(q)^{-1} \tau - k_M k_C \hat{M}(q)^{-1} \hat{C}(\dot{q}, q)\dot{q} - \ddot{q}_d + K\dot{e}_1]
\end{aligned} \tag{20}$$

Step 3: We set

$$\begin{cases} a = {k_M}^{-1} \\ b = k_M k_C \end{cases} \tag{21}$$

and define

$$\begin{cases} \tilde{a} = a - \hat{a} \\ \tilde{b} = b - \hat{b} \end{cases} \tag{22}$$

where $\hat{a}$ and $\hat{b}$ denote the estimation of a and b, respectively. Then, the derivative of $\tilde{a}$ and $\tilde{b}$ can be obtained:

$$\begin{cases} \dot{\tilde{a}} = \dot{a} - \dot{\hat{a}} = -\dot{\hat{a}} \\ \dot{\tilde{b}} = \dot{b} - \dot{\hat{b}} = -\dot{\hat{b}} \end{cases} \tag{23}$$

Herein, an adaptive law is proposed to adjust the values of unknown parameters $\hat{a}$ and $\hat{b}$, and the third Lyapunov function is chosen as

$$\begin{aligned}
V_3 &= V_2 + \frac{|k_M|}{2\eta} \tilde{a}^2 + \frac{1}{2\gamma} \tilde{b}^2 \\
&= (\frac{1}{2}\lambda^T \lambda + \frac{1}{2}) e_1^T e_1 + \lambda e_1^T e_2 + \frac{1}{2} e_2^T e_2 + \frac{|k_M|}{2\eta} \tilde{a}^2 + \frac{1}{2\gamma} \tilde{b}^2 \\
&= e^T B e + \frac{|k_M|}{2\eta} \tilde{a}^2 + \frac{1}{2\gamma} \tilde{b}^2
\end{aligned} \tag{24}$$

where η and γ are positive constants; $e = \begin{bmatrix} e_1 & e_2 \end{bmatrix}^T$; $B = \begin{bmatrix} \frac{1}{2}\lambda^2 + \frac{1}{2} I & \frac{1}{2}\lambda \\ \frac{1}{2}\lambda & \frac{1}{2} I \end{bmatrix}$.

Then the derivative of V_3 is

$$\begin{aligned}
\dot{V}_3 &= \dot{V}_2 - \frac{|k_M|}{\eta} \tilde{a}\dot{\hat{a}} - \frac{1}{\gamma} \tilde{b}\dot{\hat{b}} \\
&= e_1^T e_2 - e_1 K e_1 + s^T [\lambda (e_2 - K e_1) + k_M \hat{M}(q)^{-1} \hat{T}_c - k_M \hat{M}(q)^{-1} \tau - b \hat{M}(q)^{-1} \hat{C}(\dot{q}, q)\dot{q} - \ddot{q}_d + K\dot{e}_1] \\
&- \frac{|k_M|}{\eta} \tilde{a}\dot{\hat{a}} - \frac{1}{\gamma} \tilde{b}\dot{\hat{b}} \\
&= e_1^T e_2 - e_1 K e_1 + s^T [\lambda (e_2 - K e_1) + k_M \hat{M}(q)^{-1} \hat{T}_c - k_M \hat{M}(q)^{-1} \tau - \hat{b} \hat{M}(q)^{-1} \hat{C}(\dot{q}, q)\dot{q} - \ddot{q}_d + K\dot{e}_1] \\
&- \frac{|k_M|}{\eta} \tilde{a}\dot{\hat{a}} - \frac{1}{\gamma} \tilde{b}(\dot{\hat{b}} + \gamma s^T \hat{M}(q)^{-1} \hat{C}(\dot{q}, q)\dot{q})
\end{aligned} \tag{25}$$

Select the adaptive control rules as:

$$\begin{cases} \dot{\hat{a}} = -sign(k_M)\eta s^T \tau_c - \eta\zeta\hat{a} \\ \dot{\hat{b}} = -\gamma s^T \hat{M}(q)^{-1}\hat{C}(\dot{q},q)\dot{q} - \gamma\sigma\hat{b} \end{cases} \tag{26}$$

Then the control law is chosen as:

$$\hat{T}_c = \hat{a}\hat{M}(q)\tau_c \tag{27}$$

where $\tau_c = -hs - \lambda(e_2 - Ke_1) + \hat{b}\hat{M}(q)^{-1}\hat{C}(\dot{q},q)\dot{q} + \ddot{q}_d - K\dot{e}_1 - s\left\|\hat{M}(q)^{-1}\right\|^2$ and $\|\cdot\|$ denotes the second norm of a matrix; ζ and σ are positive constants; $h \in R^{3\times 3}$ is a positive definite diagonal coefficient matrix.
Here, assuming

$$\|k_M\tau\| \le \bar{\tau} \tag{28}$$

where $\|\cdot\|$ denotes the second norm of a vector.
Substituting Eq. (26), Eq. (27), along with Eq. (21) and Eq. (28) into the $\dot{V}_3$, then the $\dot{V}_3$ can be rewritten as

$$\begin{aligned} \dot{V}_3 &= e_1^T e_2 - e_1 K e_1 + s^T(k_M\hat{a} + k_M\tilde{a})\tau_c \\ &\quad + s^T[\lambda(e_2 - Ke_1) - k_M\hat{M}(q)^{-1}\tau - \hat{b}\hat{M}(q)^{-1}\hat{C}(\dot{q},q)\dot{q} - \ddot{q}_d + K\dot{e}_1] + |k_M|\,\zeta\tilde{a}\hat{a} + \sigma\tilde{b}\hat{b} \\ &= e_1^T e_2 - e_1 K e_1 + s^T\tau_c \\ &\quad + s^T[\lambda(e_2 - Ke_1) - k_M\hat{M}(q)^{-1}\tau - \hat{b}\hat{M}(q)^{-1}\hat{C}(\dot{q},q)\dot{q} - \ddot{q}_d + K\dot{e}_1] + |k_M|\,\zeta\tilde{a}\hat{a} + \sigma\tilde{b}\hat{b} \\ &= e_1^T e_2 - e_1 K e_1 - s^T hs - s^T s\left\|\hat{M}(q)^{-1}\right\|^2 - s^T\hat{M}(q)^{-1}k_M\tau + |k_M|\,\zeta\tilde{a}\hat{a} + \sigma\tilde{b}\hat{b} \\ &\le e_1^T e_2 - e_1 K e_1 - s^T hs - s^T s\left\|\hat{M}(q)^{-1}\right\|^2 + \left\|s^T\hat{M}(q)^{-1}\right\|^2 + \frac{1}{4}\|k_M\tau\|^2 + |k_M|\,\zeta\tilde{a}\hat{a} + \sigma\tilde{b}\hat{b} \\ &\le e_1^T e_2 - e_1 K e_1 - s^T hs - s^T s\left\|\hat{M}(q)^{-1}\right\|^2 + \|s\|^2\left\|\hat{M}(q)^{-1}\right\|^2 + \frac{1}{4}\bar{\tau}^2 + |k_M|\,\zeta\tilde{a}\hat{a} + \sigma\tilde{b}\hat{b} \\ &= e_1^T e_2 - e_1 K e_1 - s^T hs + \frac{1}{4}\bar{\tau}^2 + |k_M|\,\zeta\tilde{a}\hat{a} + \sigma\tilde{b}\hat{b} \\ &= -e_1^T A e_1 + \frac{1}{4}\bar{\tau}^2 + |k_M|\,\zeta\tilde{a}\hat{a} + \sigma\tilde{b}\hat{b} \end{aligned} \tag{29}$$

where

$$A = \begin{bmatrix} K + \lambda^T h\lambda & h\lambda - \frac{1}{2}I \\ h\lambda - \frac{1}{2}I & h \end{bmatrix}$$

By choosing proper K, λ and h, A can be a positive definite matrix.
Define

$$c_1 = \frac{\lambda_{\min}(A)}{\lambda_{\max}(B)} \tag{30}$$

where $\lambda_{\min}(A)$ is the minimum eigenvalue of matrix A; $\lambda_{\max}(B)$ is the maximal eigenvalue of matrix B. Then

$$\begin{aligned} c_1 e^T B e &\le c_1\lambda_{\max}(B)e^T e \\ &= \lambda_{\min}(A)e^T e \\ &\le e^T A e \end{aligned} \tag{31}$$

Further, we can obtain

$$\begin{aligned} \sigma\tilde{b}\hat{b} &= \sigma\tilde{b}(b - \tilde{b}) \\ &= -\sigma\tilde{b}^2 + \sigma\tilde{b}b \\ &\le -\sigma\tilde{b}^2 + \frac{1}{2}\sigma\tilde{b}^2 + \frac{1}{2}\sigma b^2 \\ &= -\frac{1}{2}\sigma\tilde{b}^2 + \frac{1}{2}\sigma b^2 \\ &= -c_2\frac{1}{2\gamma}\tilde{b}^2 + \frac{1}{2}\sigma b^2 \end{aligned} \tag{32}$$

where $c_2 = \gamma\sigma$. In a similar way

$$\begin{aligned} |k_M|\,\zeta\tilde{a}\hat{a} &\le -\frac{1}{2}\,|k_M|\,\zeta\tilde{a}^2 + \frac{1}{2}\,|k_M|\,\zeta a^2 \\ &= -c_3\frac{|k_M|}{2\eta}\tilde{a}^2 + \frac{1}{2}\,|k_M|\,\zeta a^2 \end{aligned} \tag{33}$$

where $c_3 = \eta\zeta$. Select $c = \min(c_1, c_2, c_3)$, the Eq. (29) can be transformed as

$$\dot{V}_3 \le -cV_3 + d \tag{34}$$

where $d = \frac{1}{4}\bar{\tau} + \frac{1}{2}\sigma b^2 + \frac{1}{2}\,|k_M|\,\zeta a^2$. Solving the non-homogeneous linear differential inequation Eq. (34), we can obtain

$$\begin{aligned} 0 \le V_3 &\le e^{-ct}V_3(0) + \int_0^t (e^{-c(t-\tau)}d)d\tau \\ &= \frac{c}{d} + (V_3(0) - \frac{d}{c})e^{-ct} \end{aligned} \tag{35}$$

It is obvious that

$$\lim_{t\to\infty} V_3(t) = \frac{c}{d} \tag{36}$$

This can be achieved by choosing the appropriate values of K, λ, h, γ, σ, η and ζ. As a result, the stability of the proposed adaptive backstepping sliding mode control system can be guaranteed.

IV. Simulations

Since the modeling error and the disturbance are key factors in improving the trajectory tracking performance, simulations are carried out to evaluate the proposed control scheme mainly in terms of these two aspects.

The desired trajectory is

$$q(t) = \begin{bmatrix} q_1(t) \\ q_2(t) \\ q_3(t) \end{bmatrix} = \begin{bmatrix} (\pi/12)\sin(2\pi t) \\ 0.1t\cos(\pi t) \\ 0.5\pi t \end{bmatrix}, t \in [0, 3] \tag{37}$$

The modeling error is set as

$$\Delta M(q) = m \times [M(q) + R_M \times M(q)] \tag{38}$$

$$\Delta C(\dot{q}, q) = m \times [C(\dot{q}, q) + R_M \times C(\dot{q}, q)] \tag{39}$$

$$\tau_T = \begin{bmatrix} 0.002 & 0.001 & 0.002 \end{bmatrix} \tag{40}$$

where m is the coefficient of the modeling error; R_M is a random matrix whose elements are randomly distributed in (0 1).

The external disturbance is set as

$$\tau_d = r \times \begin{bmatrix} \cos(\pi t) & sin(-\pi t) & sin(2\pi t) \end{bmatrix} \tag{41}$$

where r is randomly distributed in (0.03 0.03).

The load torque is set as

$$\tau_l = L \times \begin{bmatrix} 0.05 & 0.05 & 0.05 \end{bmatrix} \tag{42}$$

where L is the coefficient of the load torque.

Herein, the simulations in Section IV-A and Section IV-B are conducted in the condition where the desired trajectory q_d, the torque error τ_T and the external disturbance τ_d are all the same. The difference is that the first simulation is performed with varying modeling errors and a fixed load torque, while the second one is performed with different loads and a fixed coefficient of the model error.

Both the unknown parameters (k_M, k_C) in the dynamic model should be close to 1. According to Eq. (21), the original values of the adaptive parameters a and b are supposed to be respectively set as

$$\begin{cases} a(0) = 1 \\ b(0) = 1 \end{cases} \tag{43}$$

To ensure the convergence and robustness of the proposed control scheme, the controller gain matrices are set as

$$\begin{cases} K = diag\begin{bmatrix} 20 & 20 & 20 \end{bmatrix} \\ \lambda = diag\begin{bmatrix} 50 & 50 & 50 \end{bmatrix} \\ h = diag\begin{bmatrix} 50 & 50 & 50 \end{bmatrix} \end{cases} \tag{44}$$

The parameters of the adaptive controller are set as

$$\begin{cases} \eta = 10 \\ \gamma = 10 \\ \sigma = 10 \\ \zeta = 10 \end{cases} \tag{45}$$

Especially, the parameters of the compared backstepping controller are the same as that of the proposed hybrid controller.

A. Trajectory tracking in the presence of different modeling errors

In the first simulation, we set the coefficient of the load torque L as 1 ($L = 1$) and then vary the coefficient of the modeling error m from 0 to 0.3.

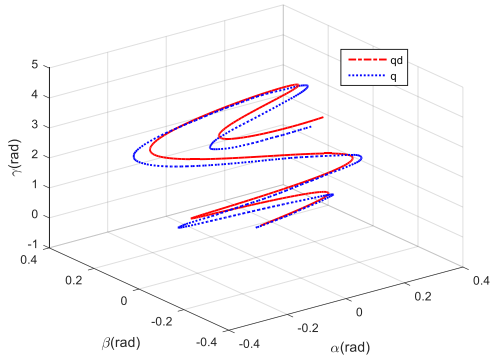

(a) Tracking performance with PD control

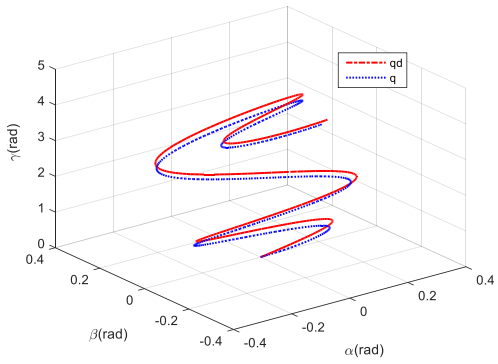

(b) Tracking performance with backstepping control

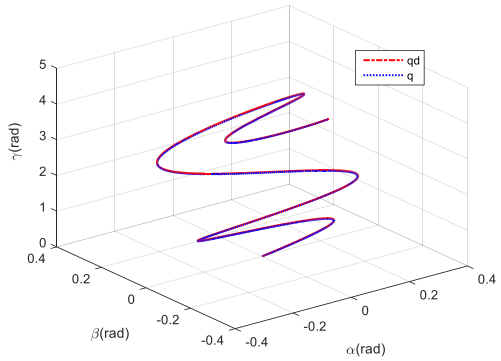

(c) Tracking performance with the proposed control

Fig. 4. The trajectory tracking comparison (L=1, m=0.3)

Fig. 4(a), Fig. 4(b) and Fig. 4(c) show the trajectory tracking performance of PD control, backstepping control and the proposed control, respectively ($L = 1$ and $m = 0.3$). Herein, q_d denotes the desired trajectory and q denotes the actual trajectory. we can see from Fig. 4(a) and Fig. 4(b) that the tracking error of both PD control and the backstepping control scheme is rather distinct, which means that the disturbance and the model error seriously affect the tracking performance. Nevertheless, it can be observed that in the case of the proposed control scheme, the actual trajectory can track the desired trajectory well and the maximum position errors of three Euler angles α, β, and γ are smaller than 0.0039, 0.0036 and 0.0035(rad), respectively.

Fig. 5 shows the convergence accuracy with variation of the coefficient of the modeling error m from 0 to 0.3. It is obvious that the convergence accuracy of the proposed control is highest among three control methods during the change of m. For example, when m is set as 0.3, under PD and backstepping control, the Euclidean norms of position errors of three Euler angles α, β, and γ are 0.4867, 0.4321, 0.4576 (rad) and 0.4405, 0.4122, 0.4269 (rad), respectively. In contrast, at the same condition, with the proposed control scheme, the corresponding Euclidean norms are 0.0832, 0.0750 and 0.0761 (rad).

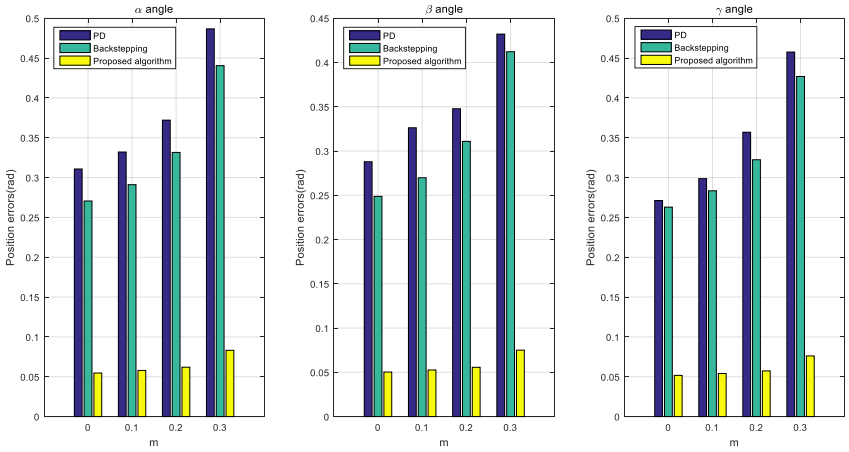

Fig. 5. The trajectory tracking accuracy (L=1 with varying m)

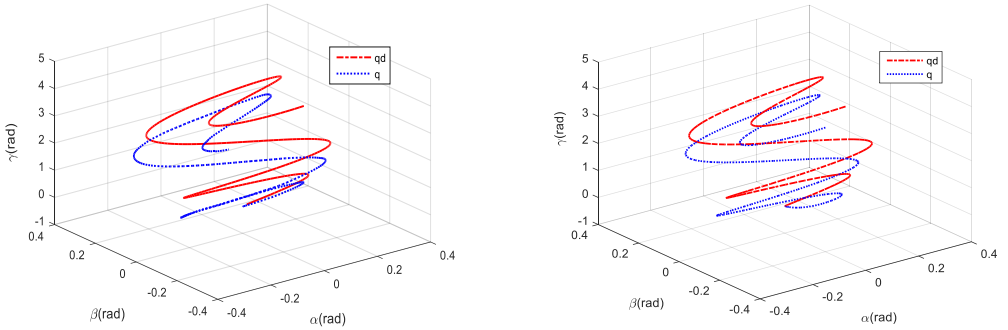

(a) Tracking performance with PD control

(b) Tracking performance with backstepping control

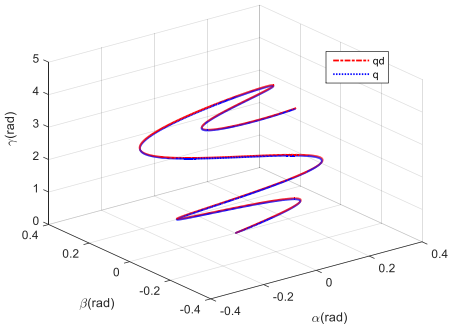

(c) Tracking performance with the proposed control

Fig. 6. The trajectory tracking comparison (m=0.2, L=4)

B. Trajectory tracking in the presence of different loads

In the second simulation, we set the coefficient of the modeling error m as 0.2 ($m = 0.2$) and then vary the coefficient of the load torque L from 0 to 4.

Fig. 6(a), Fig. 6(b) and Fig. 6(c) show the trajectory tracking performance of PD control, backstepping control and the proposed control, respectively ($L = 4$ and $m = 0.2$). We can see that there is a steady-state tracking error during the motion under the control of both PD control and backstepping control. However, with the proposed control scheme, the maximum position errors of three Euler angles α, β, and γ are smaller than 0.0057, 0.0050, and 0.0050 (rad), respectively, indicating that this approach has succeeded in compensating uncertainties during the control process.

Fig. 7 shows the convergence accuracy when the coefficient of the load torque L is varied from 0 to 4. It is clear that the convergence accuracy of the proposed control is highest among three control methods as L changes. To be specific, when L is set as 4, in the case of the control by PD and backstepping, the Euclidean norms of position errors of three Euler angles α, β, and γ are 1.3890, 1.1330, 1.2700 (rad) and 1.2760, 1.1230, 1.2500 (rad), respectively. On the contrary, under the same value of L, with the proposed control, the corresponding Euclidean norms are 0.1384, 0.1289 and 0.1315 (rad).

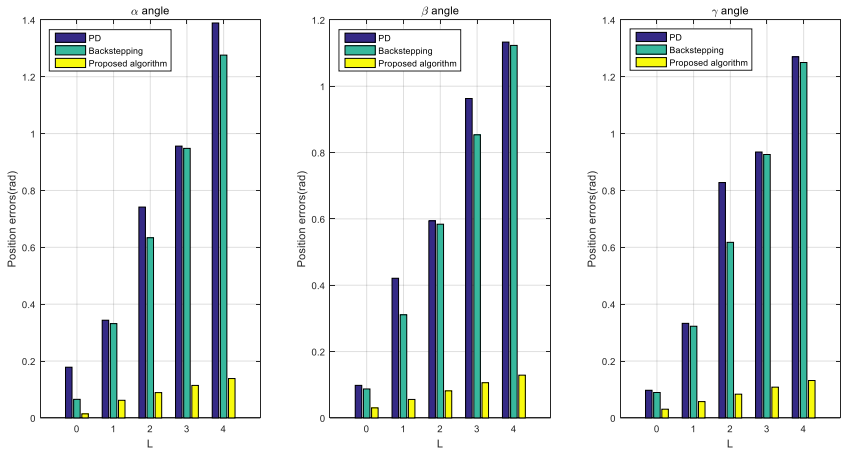

Fig. 7. The trajectory tracking accuracy (m=0.2 with varying L)

C. Trajectory tracking when the start point is in the non-original position

In the above two simulations, the PM spherical actuator can track the desired trajectory from original position (0, 0, 0) well with the proposed control scheme. For further corroborating the effectiveness and robustness of the proposed strategy, we let the actual trajectory start from a non-original position (0.4, -0.2, 1).

Fig. 8(a), Fig. 8(b) and Fig. 8(c) show the trajectory tracking performance of PD control, backstepping control and the proposed control, respectively ($L = 1$ and $m = 0.3$). We can see that even though the PM spherical actuator moves from a non-original position, the proposed control scheme can still have a better performance compared with other two control methods.

V. Experiments

Fig. 9(a) shows the experimental prototype of the spherical actuator. The rotor is supported by a passive spherical joint, which also acts as the orientation measurement system that includes an rotary encoder and a two-axis tilt sensor.

The block diagram of the control system is shown in Fig. 9(b), consisting of a PC, a digital signal processor (DSP), a field programmable gate array (FPGA), a current output device, a current sampling device and an orientation measurement module. For convenience of control and analysis, a friendly graphical user interface (GUI) program has been developed on the PC. The GUI program is not only in charge of the control mode selection, control parameter setting and command sending, but can also display the orientation information of the spherical actuator in both numeric and graphical form. The DSP is responsible for task scheduling, algorithm computing and communicating with the host computer. The FPGA performs the task of handling the data obtained from the rotary encoder and tilt sensor and driving the AD5370 and ADS8364 chips because of their capability of parallel processing . The AD5370 is a D/A chip containing digital-to-analog converters with 40 channels and 16-bit resolution. The OPA549 (a power amplifier) is chosen to achieve V/I conversion, which can convert the analog voltage signals from AD5370 into current signals. The ADS8364 is an A/D chip that can offer 6-channel output with a 16-bit A/D converting resolution.

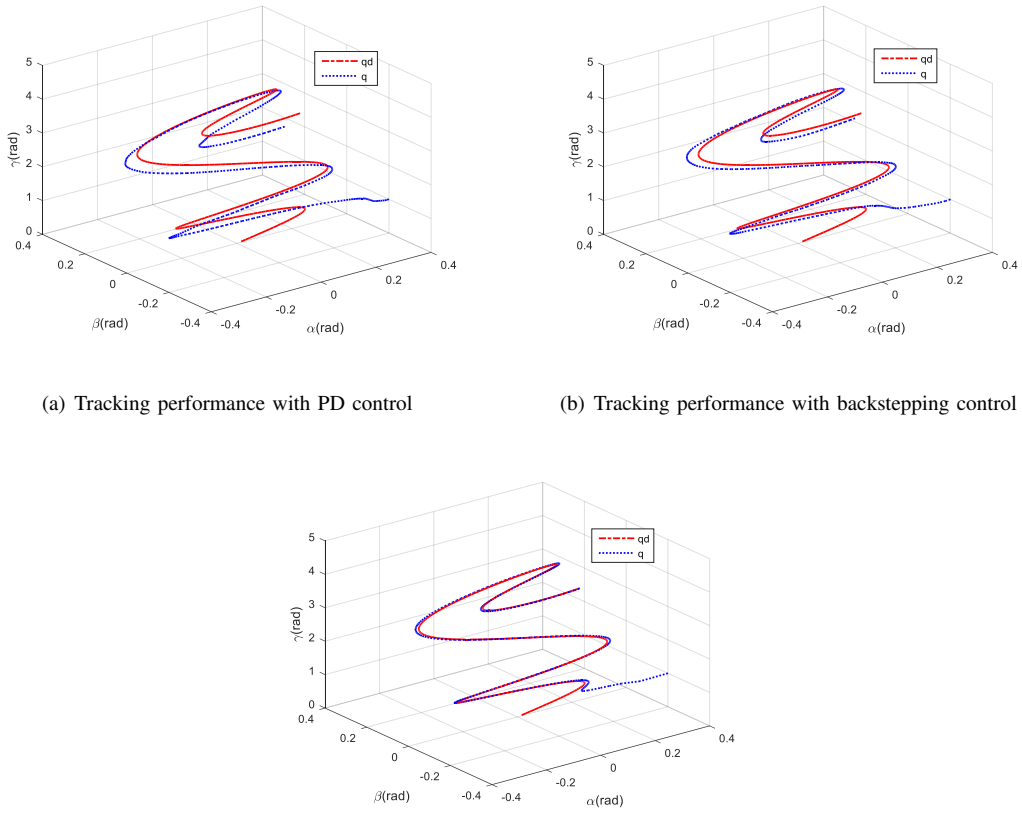

(a) Tracking performance with PD control

(b) Tracking performance with backstepping control

(c) Tracking performance with the proposed control

Fig. 8. The trajectory tracking comparison (L=1, m=0.3)

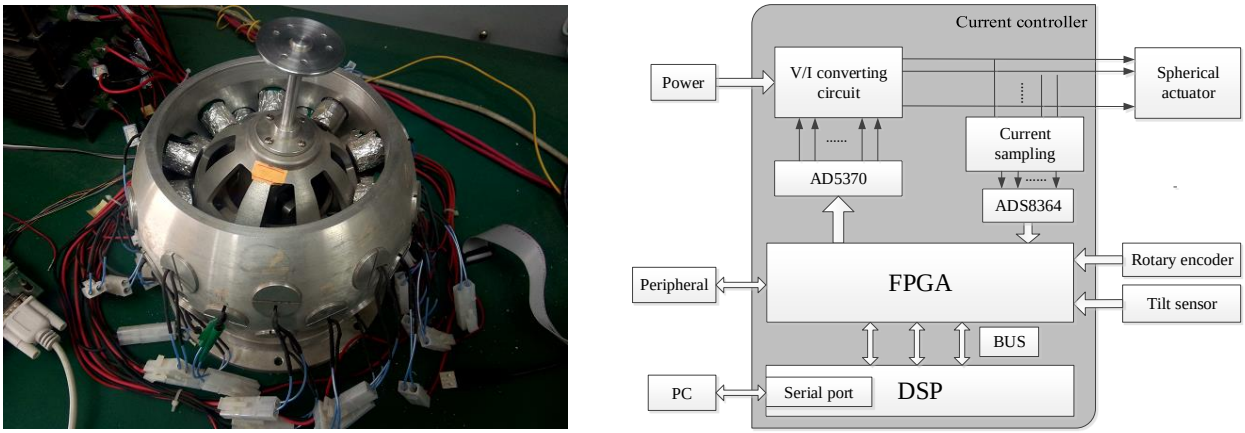

(a) Experimental prototype

(b) Block diagram of the control system

Fig. 9. Experimental prototype and block diagram of the control system

To observe the control performance preliminarily, a circular trajectory in the X-Y plane is conducted. In this experiment, a load weighting 0.2 kg is fixed on the output shaft. The desired trajectory is set as

$$q(t) = \begin{bmatrix} q_1(t) \\ q_2(t) \end{bmatrix} = \begin{bmatrix} 5\cos(\frac{2\pi t}{60} - \frac{\pi}{2}) \\ 5\sin(\frac{2\pi t}{60} - \frac{\pi}{2}) + 5 \end{bmatrix}, t \in [0, 60] \tag{46}$$

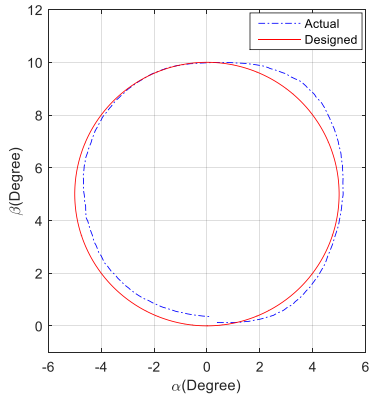

(a) Trajectory tracking performance in the X-Y plane

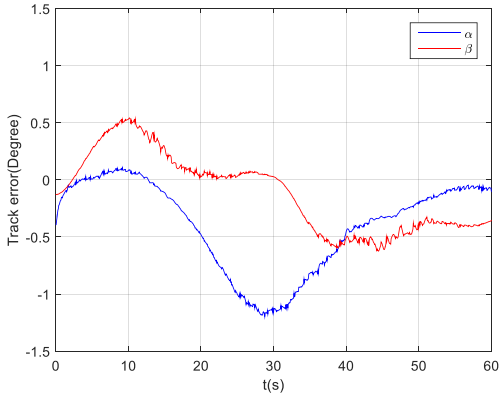

(b) The tracking error of α and β

Fig. 10. Trajectory tracking performance with the backstepping control method

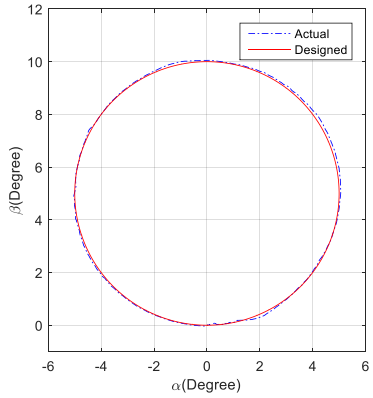

(a) Trajectory tracking performance in the X-Y plane

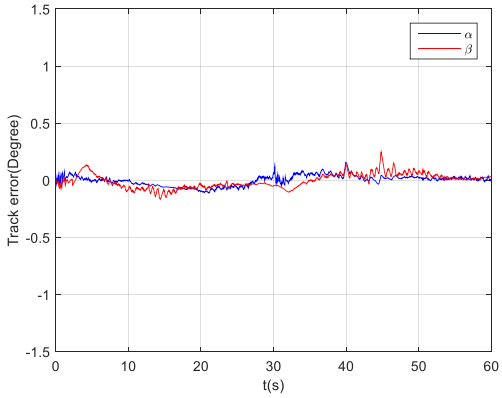

(b) The tracking error of α and β

Fig. 11. Trajectory tracking performance with the proposed control method

Fig. 10(a) shows the trajectory tracking performance of the backstepping control scheme and Fig. 10(b) shows the corresponding tracking error. It is obvious that the maximum tracking errors of both α and β are more than $0.6°$. In some positions, the tracking error of α even exceeds $1.2°$ due to the fact that the center of the rotor deviates from the center of the stator, which will cause the actual dynamic model to be different from the ideal one.

In contrast, Fig. 11(a) shows the trajectory tracking performance of the proposed control scheme and Fig. 11(b) shows the corresponding tracking error. It can be observed that the actual trajectory fits the desired trajectory extremely well and the maximum tracking errors of both α and β are smaller than $0.25°$, which indicates that uncertainties in the practical system, containing the model errors and load disturbances, have been effectively compensated.

In summary, the experimental results demonstrate that the sliding mode term can make the system robust against complicated external disturbances and the uncertainties have been successfully approximated by the adaptive law.

VI. Conclusion

This paper mainly focuses on the trajectory tracking control of a PM spherical actuator. Owing to complicated mechanical structure and electromagnetic field, there exist indefinite errors in the practical model and manifold disturbances during the control process. To cope with these uncertainties, a hybrid control scheme, combining the merits of backstepping, sliding mode and adaptive control, has been developed to improve the trajectory tracking performance of the PM spherical actuator. Firstly, the stability of the closed-loop system can be ensured by the backstepping design, which is based on the Lyapunov function. Then, the lumped disturbance, caused by the random influence, the load and the torque error, can be compensated by introducing the sliding mode term. In addition, an adaptive method is employed to adjust unknown parameters of the dynamic model in the real time. The simulation results indicate that, compared with conventional PD and backstepping control method, the proposed scheme can give much better trajectory tracking performance under different occasions, where the coefficient of m or L varies as time changes. In the end, an experimental platform, consisting of the prototype and the control system, has been developed for demonstrating the feasibility of the proposed algorithm.

Acknowledgment

This work is supported by National Natural Science Foundation of China under Grant No. 51475033.

References

B Ackermann, H Steinbusch, T Vollmer, J Wang, GW Jewell, and D Howe. A spherical permanent magnet actuator for a high-fidelity force-feedback joystick. *Mechatronics*, 14(3):327–339, 2004.

Deng Bin, Wang Jiang, and Fei Xiangyang. Synchronizing two coupled chaotic neurons in external electrical stimulation using backstepping control. *Chaos, Solitons & Fractals*, 29(1):182–189, 2006.

Weihai Chen, Liang Zhang, Liang Yan, and Jingmeng Liu. Design and control of a three degree-of-freedom permanent magnet spherical actuator. *Sensors and Actuators A: Physical*, 180:75–86, 2012.

Jonathan Hey, Tat Joo Teo, Viet Phuong Bui, Guilin Yang, and Ricardo Martinez-Botas. Electromagnetic actuator design analysis using a two-stage optimization method with coarse–fine model output space mapping. *Industrial Electronics, IEEE Transactions on*, 61(10):5453–5464, 2014.

Hoon Lee, Vadim I Utkin, and Andrey Malinin. Chattering reduction using multiphase sliding mode control. *International Journal of Control*, 82(9):1720–1737, 2009.

Kok-Meng Lee and Raye A Sosseh. Effects of fixture dynamics on back-stepping control of a vr spherical motor. In *Control, Automation, Robotics and Vision, 2002. ICARCV 2002. 7th International Conference on*, volume 1, pages 384–389. IEEE, 2002.

Kok-Meng Lee, Ronald B Roth, and Zhi Zhou. Dynamic modeling and control of a ball-joint-like variable-reluctance spherical motor. *Journal of dynamic systems, measurement, and control*, 118(1):29–40, 1996.

Zheng Li. Robust control of pm spherical stepper motor based on neural networks. *Industrial Electronics, IEEE Transactions on*, 56(8):2945–2954, 2009.

F-J Lin, P-H Shen, and S-P Hsu. Adaptive backstepping sliding mode control for linear induction motor drive. In *Electric Power Applications, IEE Proceedings-*, volume 149, pages 184–194. IET, 2002.

Faa-Jeng Lin, Chih-Kai Chang, and Po-Kai Huang. Fpga-based adaptive backstepping sliding-mode control for linear induction motor drive. *Power Electronics, IEEE Transactions on*, 22(4):1222–1231, 2007.

Tarek Madani and Abdelaziz Benallegue. Backstepping control for a quadrotor helicopter. In *Intelligent Robots and Systems, 2006 IEEE/RSJ International Conference on*, pages 3255–3260. IEEE, 2006.

Shuhei Maeda, Katsuhiro Hirata, Shohei Ikejiri, and Mingyu Tong. Feedback control of electromagnetic spherical actuator with three-degree-of-freedom. In *The XIX International Conference on Electrical Machines-ICEM 2010*, 2010.

Jadesada Maneeratanaporn, Pakpoom Patompak, Siripong Varongkriengkrai, Itthisek Nilkhamhang, and Kanokvate Tungpimolrut. Adaptive backstepping controller for triple rotary joint manipulator. In *SICE Annual Conference 2010, Proceedings of*, pages 431–435. IEEE, 2010.

Hungsun Son and Kok-Meng Lee. Open-loop controller design and dynamic characteristics of a spherical wheel motor. *Industrial Electronics, IEEE Transactions on*, 57(10):3475–3482, 2010.

Hungsun Son and Kok-Meng Lee. Control system design and input shape for orientation of spherical wheel motor. *Control Engineering Practice*, 24:120–128, 2014.

Vadim Utkin, Jürgen Guldner, and Jingxin Shi. *Sliding mode control in electro-mechanical systems*, volume 34. CRC press, 2009.

W Wang, J Wang, GW Jewell, and D Howe. Design and control of a novel spherical permanent magnet actuator with three degrees of freedom. *Mechatronics, IEEE/ASME Transactions on*, 8(4):457–468, 2003.

Changliang Xia, Chen Guo, and Tingna Shi. A neural-network-identifier and fuzzy-controller-based algorithm for dynamic decoupling control of permanent-magnet spherical motor. *Industrial Electronics, IEEE Transactions on*, 57(8):2868–2878, 2010.

Haitao Yu, Jiang Wang, Bin Deng, Xile Wei, Yanqiu Che, YK Wong, WL Chan, and KM Tsang. Adaptive backstepping sliding mode control for chaos synchronization of two coupled neurons in the external electrical stimulation. *Communications in Nonlinear Science and Numerical Simulation*, 17(3):1344–1354, 2012.

Jing Zhou, Changyun Wen, and Ying Zhang. Adaptive backstepping control of a class of uncertain nonlinear systems with unknown backlash-like hysteresis. *Automatic Control, IEEE Transactions on*, 49(10):1751–1759, 2004.